J Mater Sci (2009) 44:580–590
DOI 10.1007/s10853-008-3051-x

The influence of copper addition on microstructure and mechanical properties of thermomechanically processed microalloyed steels

S. K. Ghosh · A. Haldar · P. P. Chattopadhyay

Received: 3 July 2008 / Accepted: 15 October 2008 / Published online: 10 November 2008

Abstract The present study concerns the influence of Cu addition on the microstructural evolution and mechanical properties of directly air-cooled microalloyed thin-gauge steel. For this purpose, 1.5 wt% Cu was added to a Ti–B microalloyed steel. It is known that Ni addition to Cu-containing steel is beneficial to eliminate hot shortness caused by Cu. Therefore, the effect of Ni addition (half that of Cu in wt%) on the microstructure formation and mechanical properties has also been studied. Microstructures and mechanical properties of the directly air-cooled steels have demonstrated that addition of 1.5 wt% Cu along with 0.8 wt% Ni in Ti–B microalloyed steel results in a dual phase-like microstructure, which yielded attractive tensile strength (746 MPa) and ductility (31%). However, Cu addition deteriorated the impact toughness of the directly air-cooled Ti–B microalloyed steels.

Introduction

Attempts for improvement of strength–ductility combination of thin-gauge structural steels have resulted in a wide range of compositions and microstructures. In such steels, continuous yielding behaviour is achieved by avoiding pearlite formation in the microstructure. The low alloy ferrite-based varieties include steels designated as high strength low alloy (HSLA), dual phase (DP), transformation-induced plasticity (TRIP), complex phase (CP), etc. [1, 2]. In low alloy steels, necessary austenite hardenability is achieved through partitioning of alloying elements in austenite at the intercritical temperature range. The high alloy varieties are based on austenitic microstructures like twining-induced plasticity (TWIP) steel and light weight steels with induced plasticity (L-IP) steel [3, 4]. While high alloy steels are expensive, the strength of low alloy steels are limited due to the presence of soft ferrite in the microstructures. The strength–ductility combination of the low alloy steels may be enhanced by improving the strength of ferrite through incorporating additional strengthening process like age hardening of ferrite by addition of Cu. However, ageing does not offer any benefit in steel subjected to intercritical annealing for achieving austenite hardenability as in the cases of DP or TRIP steels because age hardening element forms coarse precipitates at the intercritical temperature and does not contribute to the mechanical properties. Therefore, the attempt of incorporating age hardening in hot-rolled steels calls for continuous cooling without intercritical annealing. Achieving continuous yielding behaviour in such steels demands adequate austenite hardenability to suppress pearlite formation during continuous cooling. Earlier, it has been demonstrated that addition of microalloying elements such as Ti, B is effective in improving the strength of HSLA steels [5]. Moreover, air-cooling of the hot-rolled steel containing adequate amount of microalloying elements formed bainitic phases [6] in the form of islands in the grain boundary and triple point regions of ferrite grains giving rise to dual phase-like microstructure [7]. The presence of adequate amount (1.0–1.5 wt%) of Cu in low alloy steel has been found to be useful for retarding $\gamma \rightarrow \alpha$ transformation [8], and in microalloyed steels, Cu addition contributes to the

S. K. Ghosh (✉) · P. P. Chattopadhyay
Department of Metallurgy and Materials Engineering, Bengal Engineering and Science University, Shibpur, Howrah 711 103, India
e-mail: skghosh@metal.becs.ac.in

A. Haldar
R & D Division, Tata Steel Limited, Jamshedpur 831 001, India

expansion of non-crystallisation region by solute drag effect [9]. Precipitation of Cu in directly air-cooled steels has also been found to be beneficial for improving the strength when the precipitates are fine and well distributed [10]. Therefore, addition of suitable amount of Cu in microalloyed steels may be useful to achieve attractive strength–ductility combination with continuous yielding behaviour in steels obtained by direct air-cooling after hot rolling.

Completion of hot rolling at intercritical region forms deformed and un-deformed ferrite in the microstructure. While finer precipitation of Cu in deformed ferrite contributes to strengthening, undeformed ferrite is relatively coarser precipitates formed therein is relatively softer and contribute to ductility. Further a good amount of finer precipitates formed at the lower temperature are distributed within the low temperature transformation product of austenite and give rise to additional strengthening.

It may be mentioned here that addition of Cu necessitates simultaneous addition of Ni by an amount half that of Cu (in wt%) for suppressing the hot shortness caused by the formation of low melting Cu–Fe eutectic phase [11].

Taking the aforesaid facts into consideration, the present study attempts to develop dual phase-like microstructures by direct air-cooling of Cu-added Ti–B microalloyed steel. The continuous cooling transformation diagram of Ti–B, Cu (1.5 wt%)-Ti–B and Cu (1.5 wt%)-Ni (0.8 wt%)-Ti–B steels have been constructed to understand a priori the phase evolution in the steels under different continuous cooling conditions. The directly air-cooled Cu–Ni–Ti–B steel has yielded the microstructure and mechanical properties comparable with the high strength varieties of dual phase steels.

Experimental

The alloys were prepared in a laboratory scale induction-melting furnace (5 kg capacity). The ingots were cast into a preheated cast iron mould with approximately 50 mm square section. Chemistry of the steels was analysed using an Optical Emission Spectrometer (SPECTROLAB – M8). The cast ingots after homogenisation at 1200 °C for 120 min in a resistance-reheating furnace were forged into bars of 12.5 mm × 12.5 mm section. The forged bars were soaked at 1200 °C and hot-rolled down to a thickness of approximately 6 mm in three passes in a laboratory scale two high rolling mill (10 HP) with finish rolling temperature (FRT) of 750 °C. The FRT was determined in a manner such that approximately 10% deformation can be accomplished within the two-phase ($\gamma + \alpha$) region. After completion of rolling, the samples were cooled in air. The steels samples were subjected to dilatometric study using quartz-tipped linear variable displacement transducer (LVDT) type dilatometer with Gleeble 1500 thermomechanical simulator.

The microstructures of the samples were examined using the optical (Versamet – II) and scanning electron (SEM: JEOL, JSM-5510) microscope operated at 20 kV. For this purpose, different etchants with varying compositions like nital, picral and Vilella's reagent were tried. For Cu-bearing samples, while etching with nital (2–5%) resulted in formation of pits within a very short time, the contrast developed after etching with picral was not adequately satisfactory. Etching with Vilella's reagent (1 g picric acid, 5 mL hydrochloric acid and 95 mL ethyl alcohol) [12] yielded the desired clarity of microstructure. Transmission electron microscopy (TEM) of samples was performed (PHILIPS, CM – 200 with EDAX microscope operated at 200 kV) along with selected area diffraction and energy dispersive X-ray spectroscopic analysis (EDS) as and when essential. Discs 3 mm in diameter of TEM samples were punched out of the thin strips (<0.1 mm) and were electrolytically polished at a temperature >12 °C using a mixture of 90% acetic acid and 10% perchloric acid by a twin-jet electropolisher set at a voltage of 60 V. Hardness values presented as Vickers hardness number (VHN) were measured using 2 kg load.

Tensile specimens with flat surface along the plane of rolling were tested using an Instron – 4204 testing machine as per ASTM Standard (ASTM: Vol. 03.01: E8 M – 96). The error in yield strength (YS) and ultimate tensile strength (UTS) measurement was noted as $\sim\pm3\%$ and the same for percent elongation was $\sim\pm5\%$.

Charpy V notch impact testing of the samples (rolling direction) was conducted at 25, 0, −25 and −50 °C temperatures following the ASTM standard (ASTM: Vol. 03.01: E23 – 96). The sub-size samples were prepared with 55 mm × 5 mm × 5 mm dimensions. The average of three consistent test results was recorded as the impact value for the corresponding samples. The error for Charpy V notch value was approximately $\sim\pm10\%$.

Results and discussion

The results of the spectroscopic analysis of the steels are presented in Table 1. The presence of hyper-stoichiometric amount of Ti (i.e., Ti:N $\cong$ 3.41) [13] in the present Ti and B microalloying steels indicates that B is available in the elemental form for the improvement of austenite hardenability. In the present study, the effects of Cu addition with and without Ni has been assessed against the Ti–B microalloyed steel prepared without Cu and Ni addition.

Transformation under continuous cooling conditions

Figures 1, 2, 3 present the CCT diagrams for the Ti–B microalloyed steel, 1.5 wt% Cu-added Ti–B microalloyed

Table 1 Chemical composition of the investigated steels (wt%)

Steel identification	C	Mn	Si	S	P	Ti	B	Cu	Ni	N
Ti –B	0.04	1.60	0.49	0.021	0.013	0.028	0.0009	–	–	0.0056
1.5 Cu–Ti–B	0.04	1.69	0.57	0.021	0.013	0.032	0.0013	1.54	–	0.0080
1.5 Cu–Ti–B–Ni	0.04	1.68	0.53	0.020	0.013	0.032	0.0012	1.55	0.79	0.0058

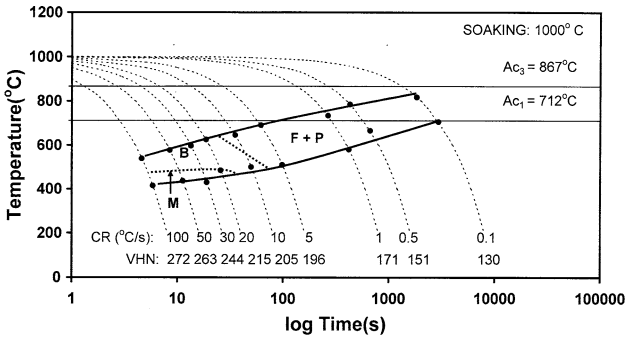

Fig. 1 CCT diagram for Ti- and B- containing steel. F: Ferrite, P: Pearlite, B: Bainite, M: Martensite

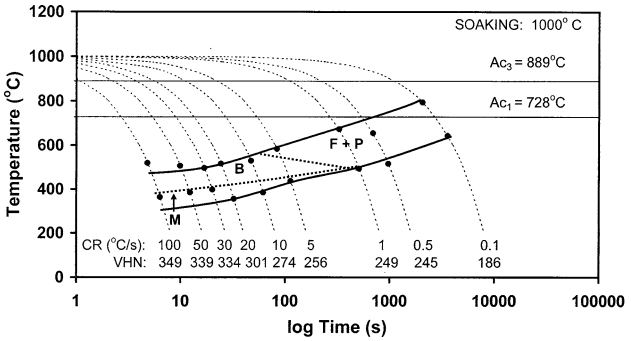

Fig. 2 CCT diagram for 1.5 wt% Cu-containing Ti–B microalloyed steel

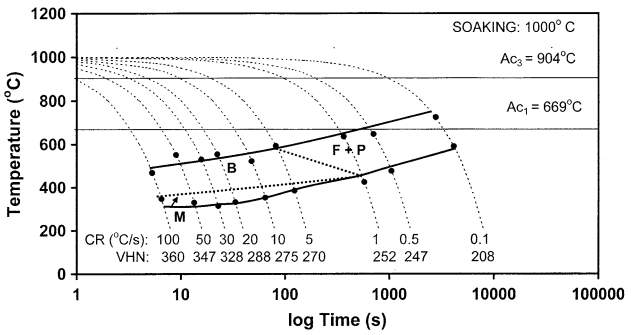

Fig. 3 CCT diagram for 1.5 Cu–Ni–Ti–B steel

steel and Ni-added 1.5 Cu–Ti–B steels, respectively, which reveals formation of the microstructure as the cooling rate increased from 0.1 to 100 °C/s. Solid points were measured from dilatometric data and dotted lines were determined by microhardness and metallographic observations. All diagrams exhibit multitransformation curves.

From Fig. 1, it may be noted that for cooling rates below 20 °C/s austenite transformation starts at temperatures $\geq$600 °C and finishes at temperatures $\geq$500 °C. It reveals that a notable amount of ferrite (F) and pearlite (P) is present in the Ti–B microalloyed steel cooled in the range of 0.1 to 5 °C/s, which is close to the cooling rate measured under air-cooling condition in the present study. The microstructure formed beyond 5 °C/s is predominantly bainitic (B) and devoid of pearlitic phase. Small amount of martensite (M) was observed at the cooling rate $\geq$10 °C/s and increased amount of martensite was produced by increasing the cooling rate.

Figure 2 shows that addition of 1.5 wt% Cu in Ti–B steel has lowered the transformation temperature of austenite below 600 °C for cooling rates as low as 5 °C/s. Notable amount of ferrite plus pearlite was present under a cooling rate range of 0.1 to 1 °C/s. Steel cooled at 5 °C/s contains ferritic phase without any perceptible amount of pearlite. At higher cooling rates martensitic and/or bainitic phase is predominant in the microstructure.

Figure 3 demonstrates that addition of 0.8 wt% Ni resulted in further lowering of austenite transformation start temperature. The microstructures formed at a cooling rate range of 0.1 to 1 °C/s are essentially ferrite and pearlite in nature. Bainitic phases with some martensitic islands are formed at a cooling rate $\geq$1 °C/s. At higher cooling rates $\geq$20 °C/s the microstructure comprises bainitic and martensitic phases. The results thus indicate that addition of 1.5 wt% Cu in Ti–B steel is adequately effective in lowering the austenite start temperature and in suppressing pearlite formation under cooling rates comparable with air-cooling. Addition of 0.8 wt% Ni has further reduced the austenite transformation temperature and formed dual phase-like microstructure at cooling rates comparable with air-cooling condition.

The hardness values achieved under different cooling rates for the alloys are also appended suitably in the CCT diagrams. Addition of Ti and B resulted in small improvement of hardness above a cooling rate of 10 °C/s. For the other alloys, the plateaus are attained after a cooling rate of 50 °C/s. At any given cooling rate, the hardness values vary with alloying in the order of Ti + B < Cu + Ti + B < Ni + Cu + Ti + B.

The observed variation in hardness among different alloys particularly at higher cooling rates may be attributed to the fact that addition of increased amount of Cu and the presence of Ni in the Ti–B microalloyed steel enhance the formation of low temperature transformation products. The attainment of plateau above a cooling rate of 50 °C/s for all the alloys indicates that the saturation of displacive transformation.

Microstructure evolution in directly air-cooled steel

Figure 4a and b shows the optical and scanning electron microstructures of Ti–B microalloyed sample after hot rolling followed by direct air-cooling. Optical microstructure shown in Fig. 4a reveals mixed morphology of ferrite grains along with the distribution of dark phases at the ferritic grain boundaries and triple point regions. The corresponding SEM micrograph shown in Fig. 4b reveals islands with brighter contrast and prominent signature of etching effects. In this regard, it has been demonstrated earlier that etching of multiphase steel samples results in a smooth and featureless appearance for martensite and retained austenite whereas phases containing carbides, e.g. tempered martensite, reveal a distinct etching contrast. Thus, the clear etching contrast observed in the grain boundary/triple point areas in Fig. 4b allows to identify the same as pearlitic in nature [14–16]. Figure 4c shows the TEM micrograph of Ti–B microalloyed steel sample, taken selectively from the triple point junction of polygonal ferrite grains. The micrograph reveals ferrite grains with the dislocation substructure, indicating the effect of rolling in non-recrystallisation region. Figure 4d reveals the TEM micrograph of Ti–B microalloyed steel sample selectively taken from a region at the grain boundary containing austenite decomposition product. The micrograph clearly identifies the product as the pearlitic phase formed at the grain boundary and triple points.

The optical micrograph shown in Fig. 5a reveals that the grain boundary phases in the microalloyed sample containing 1.5 wt% Cu are essentially non-pearlitic in nature. The corresponding SEM micrograph (Fig. 5b) reveals that the morphology of the austenite decomposition products are either island or acicular in nature. Occasional presence of ferritic phase with irregular boundaries is also evident. Such ferritic phase forms during the transformation of single-phase austenite to single-phase ferrite by rapid cooling in low carbon steels and has been designated as quasi-polygonal ferrite (α_q) by ISIJ Bainite Committee [17]. Figure 5c is the TEM micrograph of 1.5 wt% Cu-added Ti–B microalloyed sample which reveals the non-equiaxed ferritic grains with varying density of precipitates at the grain boundaries as well as within the ferrite grains. For the same alloy Fig. 5d reveals a mixture of lath-like and quasi-polygonal ferrite grains. The micrograph also

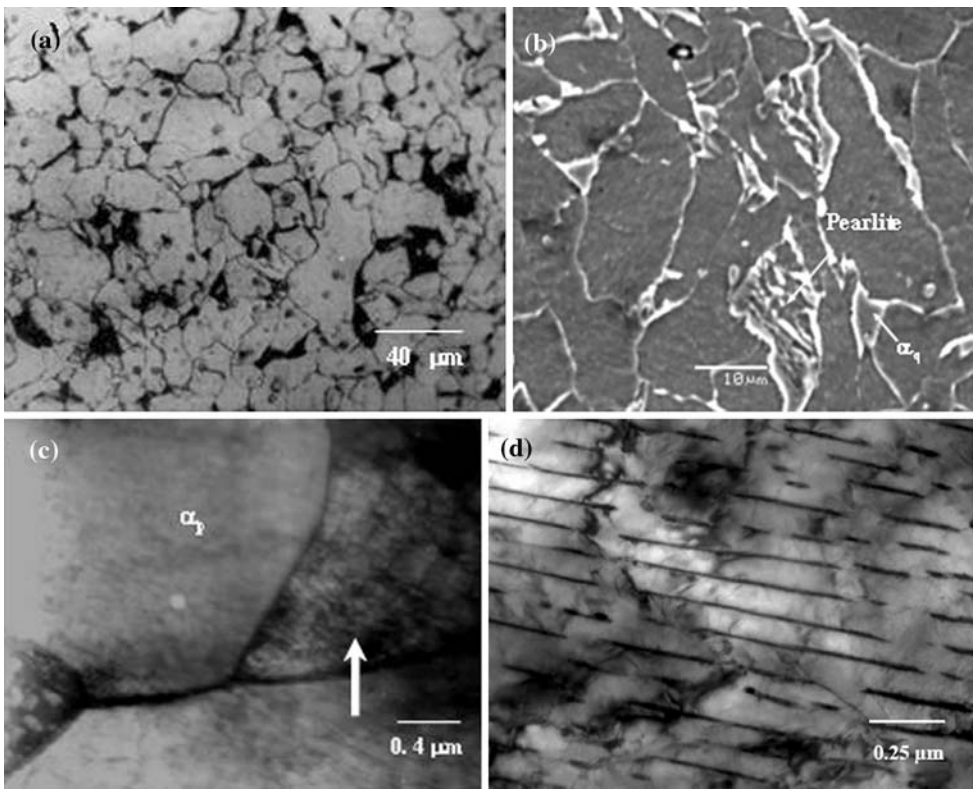

Fig. 4 **a** Optical micrograph of Ti–B microalloyed sample showing the dark pearlitic regions, **b** SEM micrograph of the same sample showing the etching effected pearlitic phases, **c** TEM micrograph revealing ferrite grains with dislocation sub-structure (arrowed) and **d** TEM micrograph showing the pearlite

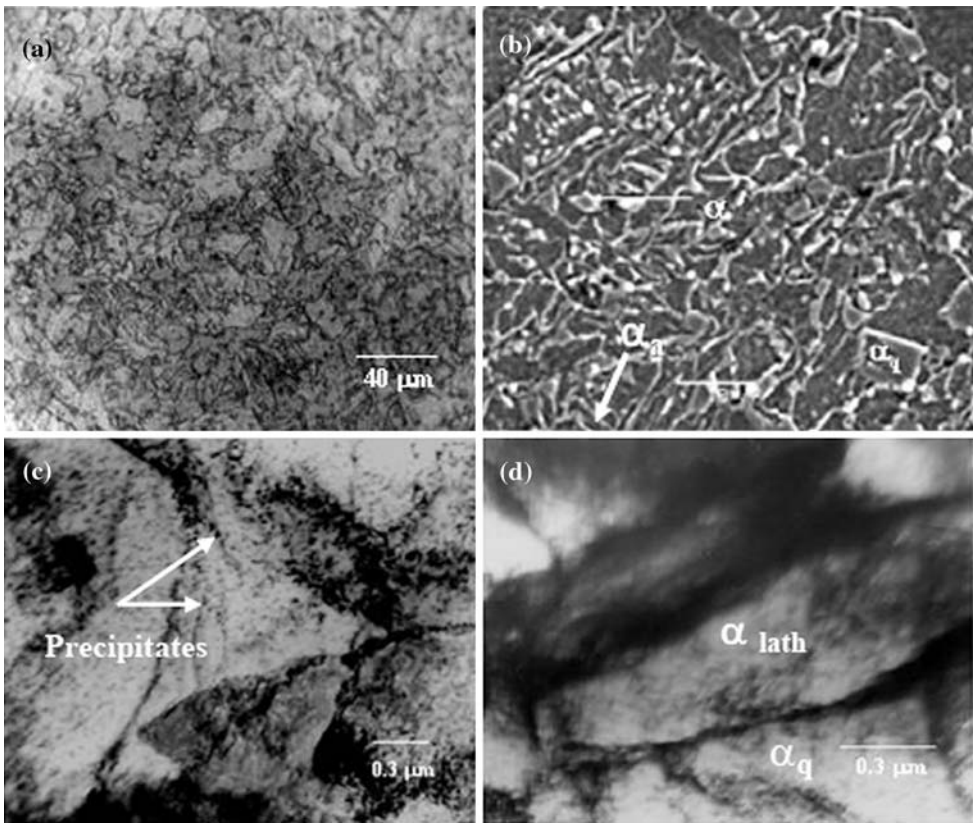

Fig. 5 **a** Optical micrograph of 1.5 Cu–Ti–B steel sample showing the fine ferritic microstructure with distribution of dark islands, **b** SEM micrograph showing the distributions of martensitic islands (α') and quasi-polygonal ferrite (α_q) and acicular ferrite (α_a), **c** TEM micrograph revealing ferrite grains with the formation of precipitate at the dislocation concentration and **d** TEM micrograph of the lath-like ferrite at the boundaries of quasi-polygonal ferrite

exhibits notable amount of dislocation density. The ferritic laths are bainitic ferrites grown under the constraints imposed by the grain boundary and dislocation tangles.

Figure 6a and b shows the effect of Ni addition on the microstructural evolution of Cu-added Ti–B microalloyed steel. The optical micrograph as shown in Fig. 6a indicates finer distribution of quasi-polygonal ferritic regions along with uniform distribution of interconnected island along the interferritic boundaries. It may particularly be emphasised that the SEM microstructure of the Ni-added sample shown in Fig. 6b reveals that the pearlitic phases along the boundaries are almost absent in the microstructure. The martensitic islands (α') comprising martensite and austenite with brighter contrast are extremely fine with island morphology. The microstructure also shows the presence of quasi-polygonal ferritic regions. Figure 6c exhibits the formation of lath-like ferrite grains in Ni-containing Cu-added Ti–B microalloyed steel. The microstructure also reveals the formation of precipitates within the ferrite lath. The lath-like phase could be either bainite (α_B^o) or martensite (α') which are indistinguishable in the present low carbon steels. From different locations of the lath, reasonable number of energy dispersive spectroscopy (EDS) plots has been obtained. One such plot, obtained from the region marked by an arrow in Fig. 6c, is shown in Fig. 6d, which confirms the presence of Cu precipitate. The micrograph taken from the same alloy from a different location shown in Fig. 6e exhibits the formation of martensite–austenite (MA) constituents comprising lath martensitic phase and austenite at the triple point.

Tensile properties

Figures 7 and 8 reveal that the steels containing Ti–B yielded the yield strength (YS), ultimate tensile strength (UTS), uniform elongation (UEL) and total elongation (TEL) values of 339 MPa, 500 MPa, 26.8% and 39%, respectively. The results also demonstrate the influence of Cu in improving the YS (437 MPa). Addition of Cu (1.5 wt%) with Ti and B improved the strength (711 MPa) with notable sacrifice in ductility (from 39% to 24%). However, the loss in ductility is significantly recovered (31%) with improvement in yield strength (515 MPa) and tensile strength (746 MPa) by the addition of Ni. The maximum strength–ductility combination (UTS × TEL) ($\sim$23 GPa%) has been achieved in Ni-containing sample.

The tensile properties obtained in the case of Ti–B steel are primarily contributed by the ferritic component of the microstructure (Fig. 4). The presence of pearlitic islands at the grain boundaries does not contribute to the deformation of ferrite as it happens due to the formation of martensitic islands in the case of dual phase steel. Addition of 1.5 wt% Cu has enhanced the strength by virtue of the formation of martensitic islands at the grain boundaries in addition to the

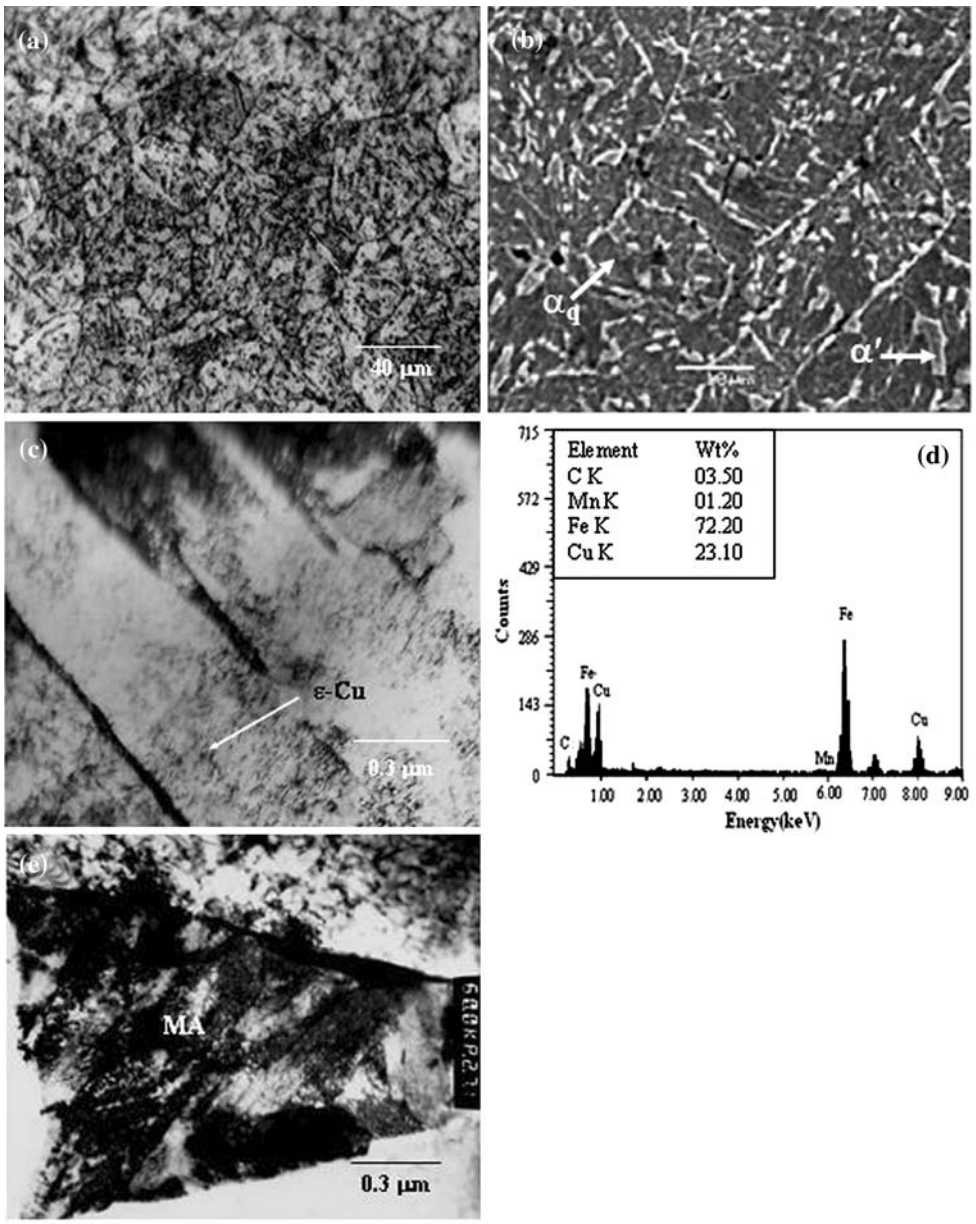

Fig. 6 **a** Fine ferritic microstructure in the optical micrograph of 1.5 Cu–Ti–B–Ni sample, **b** ferrite grains, quasi polygonal ferrite (α_q) and martensitic islands (α') in the SEM micrograph of the same sample, **c** TEM micrograph revealing ferrite laths with dislocation substructures pinned by the precipitates, **d** EDS plot and the chemical composition from the region marked by an arrow in (**c**) indicating the presence of ε-Cu precipitate and **e** MA constituent phase at the triple point region

contributions due to the precipitation of Cu and refinement of ferrite grains (Fig. 5). However, reduction of volume fraction of ferrite has reduced the ductility value. Addition of Ni has evidently widened the temperature range between Ac_3 and Ac_1 and thereby allowed considerable extent of recovery of the deformed microstructure (Fig. 6). The additional refinement achieved thereby has enhanced the strength–ductility combination in 1.5 Cu–Ti–B–Ni steel.

Work hardening behaviour of the directly air-cooled steels

The observed difference in tensile properties between 1.5 wt% Cu–Ti–B and 1.5 wt% Cu–Ni–Ti–B steels may be attributed to the work hardening behaviour of the steels. Work hardening behaviour is generally expressed by Hollomon's equation [18] that describes the true stress (σ)–true strain (ε) as:

$$\sigma = K\varepsilon^n \tag{1}$$

where n is the work hardening exponent and K is the strength coefficient. The values of n and K are determined from the slope and intercept of $\ln\sigma$ versus $\ln\varepsilon$ plot, respectively.

Figure 9 shows the Hollomon's plots of different samples indicating non-linear variation of $\ln(\sigma)$ as a function of $\ln(\varepsilon)$ for 1.5 wt% Cu–Ti–B and 1.5 wt% Cu–Ni–Ti–B steels in contrast to the Ti–B microalloyed steels which shows an approximately linear variation. Such non-

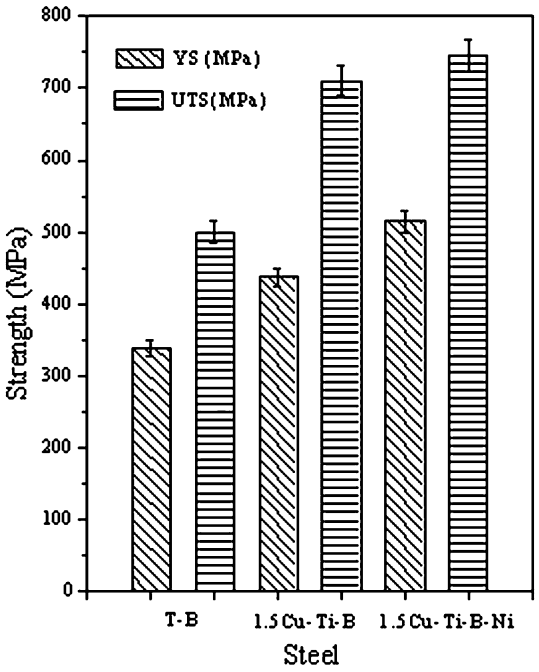

Fig. 7 Yield strength and tensile strength values of directly air-cooled steels

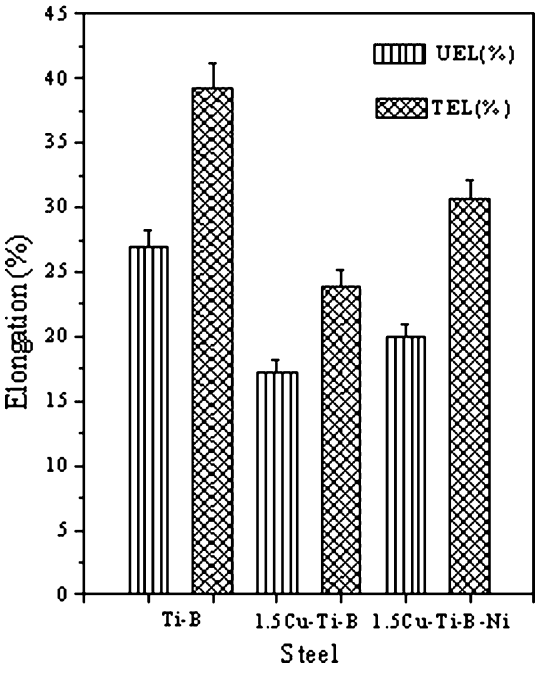

Fig. 8 Uniform elongation and total elongation values of the investigated steels

linearity in the Hollomon's plot indicates that the work hardening behaviour cannot be attributed to a single value of work hardening coefficient (n).

The non-linear Hollomon's plot obtained earlier in DP steels introduced Jaoult–Crussard (J–C) analyses of stress–strain data [19, 20] to understand the work hardening behaviour. The differential J–C analysis [21, 22] is based on the Ludwik relation [23] expressed as:

$$\sigma = \sigma_0 + k'\varepsilon^{n'} \tag{2}$$

where n' is the work hardening exponent and σ_0 and k' are the material constants. The logarithmic form of Eq. 2 after differentiation with respect to ε is

$$\ln(\mathrm{d}\sigma/\mathrm{d}\varepsilon) = \ln(k'n') + (n'-1)\ln\varepsilon \tag{3}$$

In the $\ln(\mathrm{d}\sigma/\mathrm{d}\varepsilon)$ versus $\ln\varepsilon$ plot, the slope of the line gives $(n'-1)$.

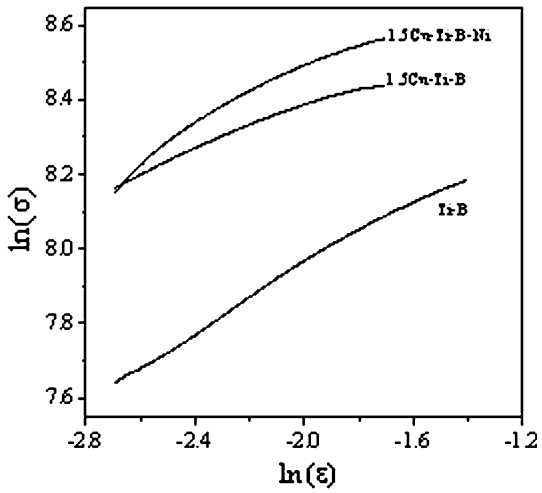

Fig. 9 Hollomon's plot of $\ln(\sigma)$ versus $\ln(\varepsilon)$ of the steels

Figure 10 shows the different stages of work hardening behaviour of 1.5 wt% Cu–Ti–B and 1.5 wt% Cu–Ni–Ti–B steels manifested by the logarithmic variation of the work hardening rate versus strain. The 1.5 wt% Cu–Ti–B steel exhibits almost continuous variation of $\ln(\mathrm{d}\sigma/\mathrm{d}\varepsilon)$ within a large range of $\ln(\varepsilon)$. However, in the cases of 1.5 Cu–Ni–Ti–B sample variation of $\ln(\mathrm{d}\sigma/\mathrm{d}\varepsilon)$ at different levels of $\ln(\varepsilon)$ clearly delineates three different stages of work hardening associated with different $(n'-1)$ values. It is also apparent that among the different stages the first stage is associated with a rapid decrease of work hardening rate with appreciable negative values of $(n'-1)$, followed by an increase in work hardening rate at the second stage and finally decrease in $(n'-1)$ value as the third stage is approached.

Continuous work hardening behaviour in the case of 1.5 wt% Cu–Ti–B steel is indicative of higher flow stress of ferrite and scarcity in mobile dislocation. In this steel the proeutectoid ferrites are mostly deformed and finer Cu precipitates formed therein during air-cooling caused effective immobilisation of the dislocations. This results in higher flow stress of ferrite and reduces plastic incompatibility among the constituent phases. Deformation in ferrite

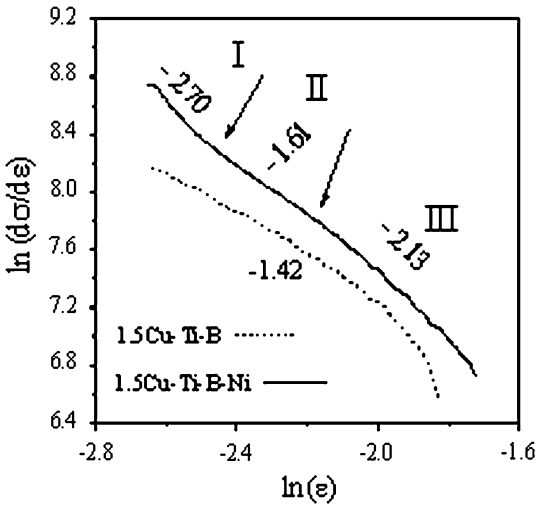

Fig. 10 Differential Jaoult–Crussard analysis of ln(dσ/dε) versus ln(ε) of the steels. Arrows indicate changes in slope and numbers represent ($n' - 1$) values

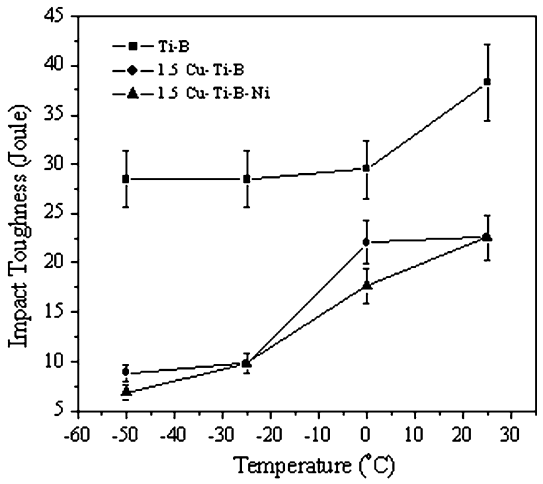

Fig. 11 Variation of Charpy impact toughness (Joule) of investigated steels with the testing temperature

continued by cutting through the precipitates restrained rapid decrease in work hardening rate over the range of strain.

In the case of 1.5 wt% Cu- and Ni-containing microalloyed steels the observed work hardening behaviour may be explained in analogy with the earlier proposition concerning three-stage work hardening of DP steels [19–22, 24]. Comparison of CCT diagrams of the steel revealed that Ni addition lowered the Ac_1 temperature (Fig. 3). Microstructure of the directly air-cooled Ni-containing steel also exhibits notable amount of undeformed proeutectoid ferrite (Fig. 6a and b). Stage I of work hardening involves plastic deformation of softer ferrite phase and only elastic deformation of martensite. The second stage (stage II) may be identified in terms of the constrained plastic flow of ferrite due to the presence of martensitic islands at the grain boundaries and triple points. At this stage, deformation of ferrite occurs at higher level of stress and involves dislocation movement, by cutting through the precipitates in deformed ferrite grains. As a result, work hardening rate decreases less rapidly. Deformation in the third stage (stage III) occurs under iso-strain condition by dynamic recovery and cross slip in ferrite and plastic deformation of harder phases like martensite and/or bainite at the grain boundaries and triple points, resulting in a decrease in the work hardening rate.

Therefore, it is apparent that while precipitation of Cu introduces continuous work hardening by constraining mobility of dislocation in deformed ferrite, the presence of a reasonable amount of undeformed ferrite in Ni-containing steel contributes to work hardening at the first and second stages of work hardening and, hence, improves the strength–ductility combination.

Impact toughness

Figure 11 presents the Charpy impact toughness for the different microalloyed steels. It is evident that the addition of Cu markedly reduced the impact properties in comparison with the Ti–B microalloyed steel within the chosen range of temperature. Marked reduction in the impact value of Cu-added samples has been noted at the sub-zero temperature range. While no distinct transition temperature range is recorded for Ti–B microalloyed sample, the Cu-added samples exhibit a distinct transition temperature range from −25 to 0 °C. In the case of Cu-added samples, the upper and lower shelf energy values remain almost unaltered. On the other hand, the Ni- and Cu-added samples exhibit a gradual reduction of energy value with the lowering of temperature. Thus, the results are indicative of deterioration in impact toughness induced by Cu addition in Ti–B microalloyed steels. Similar effect due to Cu addition has earlier been reported in the literature [25]. The deterioration in ductility in the directly air-cooled Cu-added steel may be attributed to the pinning of dislocations in the deformed ferrite by Cu precipitates.

Fractography

Figure 12a and b shows the SEM micrographs of the fracture surface obtained from the Ti and B microalloyed directly air-cooled samples subjected to Charpy impact testing at different temperatures. It is apparent that there is a transition of fracture behaviour from completely ductile to a quasi-brittle nature. While Fig. 12a reveals predominantly ductile fracture with varying dimple size and depth, Fig. 12b presents a typical quasi-brittle fracture surface with a notable appearance of shear links along the shallower cavity walls and occasional appearance of cleavage patches.

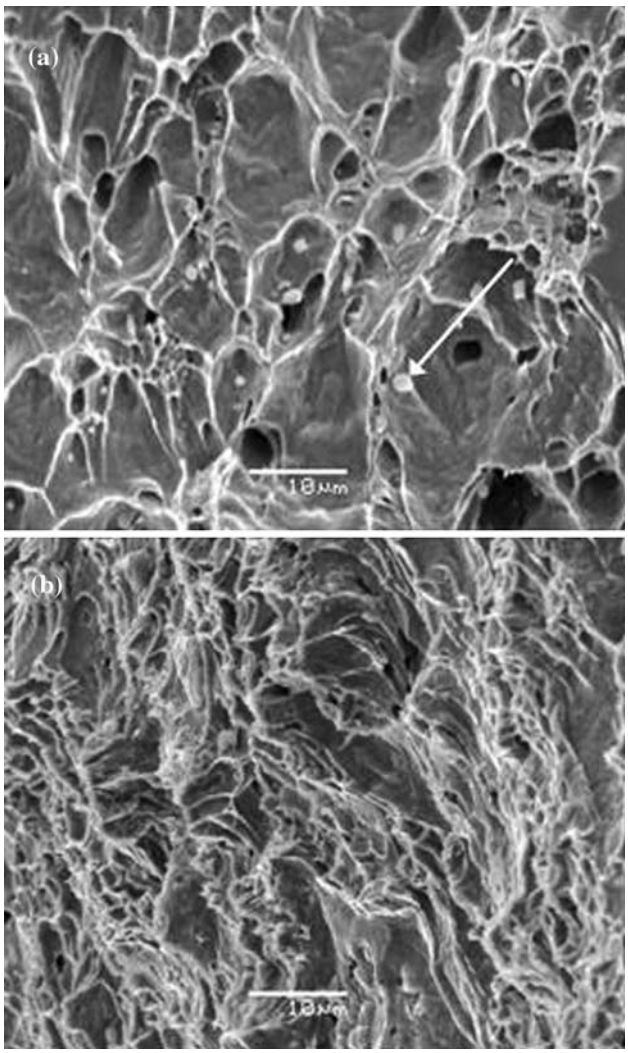

Fig. 12 SEM fractograph of the Ti–B microalloyed sample tested at **(a)** 25 °C and **(b)** −50 °C. Note the transition of the fracture mode from completely ductile to quasi-brittle nature. The particle marked by an arrow is identified as MnS

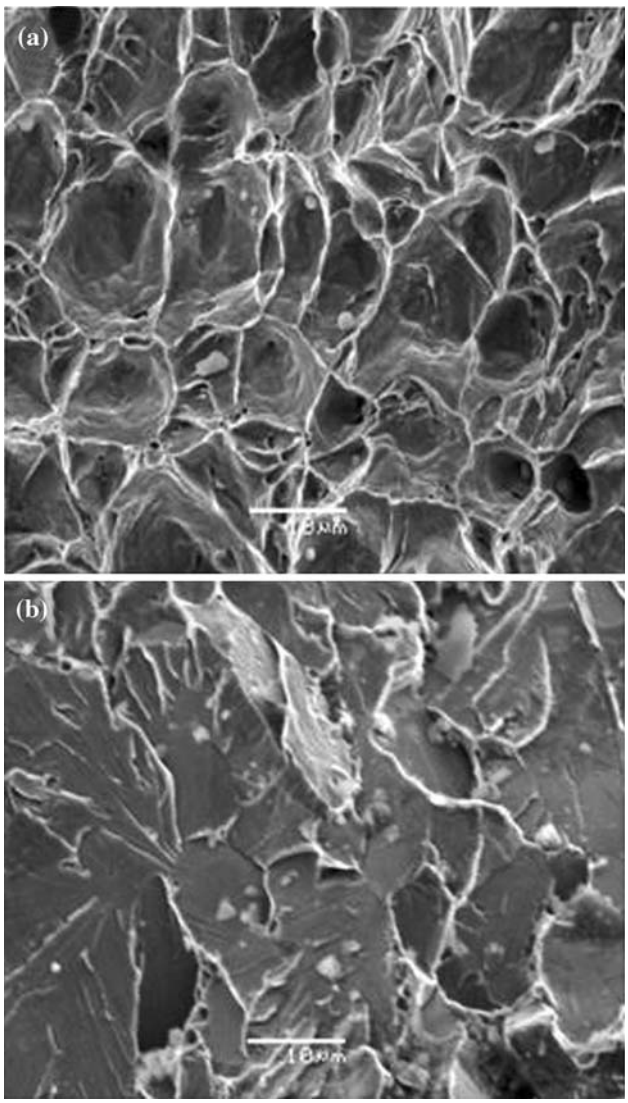

Fig. 13 SEM fractograph of the 1.5 wt% Cu-added Ti–B steel sample tested at **(a)** 25 °C and **(b)** −50 °C. Note the transition of the fracture mode from a predominantly ductile to brittle nature

Figure 13a and b shows the SEM fractographs of Cu (1.5 wt%)-added Ti–B microalloyed steel samples. Figure 13a reveals a predominantly ductile fracture with a notable presence of shear link at the inter- and intra-dimple walls. The diameters of the dimples are relatively larger than that of the Ti–B microalloyed sample. Figure 13b reveals typical brittle nature of fracture surface with a distribution of flat cleavage facets.

Figures 14a and b shows the SEM fractographs of Ni-and Cu (1.5 wt%)- added Ti–B microalloyed directly air-cooled samples. The transition of fracture behaviour is from completely ductile to a quasi-brittle nature. Figure 14a reveals predominantly ductile fracture with a range of distribution of dimple size and depth with an occasional appearance of spherical particles at the dimple root. Figure 14b demonstrates faceted surfaces typical of brittle fracture.

It may be recorded that the fractographs reveal reasonably low level of inclusion content for the present alloys and inclusions on fracture surfaces were identified as MnS and Al_2O_3.

The fractographic features of the samples are in conformance with the corresponding impact energy values. Ti–B microalloyed steel has yielded higher impact values than the Cu-bearing steels (Fig. 11) over the whole range of temperature of impact testing. This is in agreement with the observation that after testing at −50 °C temperature, fractograph obtained from Ti–B microalloyed sample is of a quasi-brittle nature (Fig. 12b) in contrast with the brittle fracture of Cu-bearing steels (Figs. 13b and 14b). Brittle fracture behaviour for Cu-bearing steels may be attributed to the presence of Cu precipitates in deformed ferrite matrix

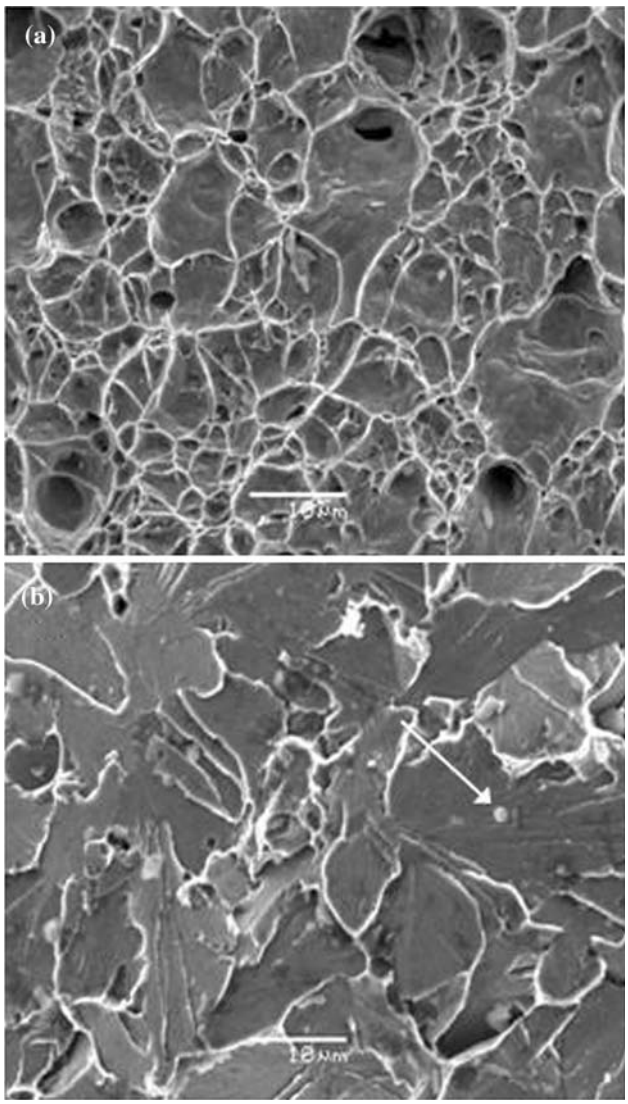

Fig. 14 SEM fractograph of the Ni- and 1.5 wt% Cu-added Ti–B steel tested at **(a)** 25 °C and **(b)** −50 °C. Note the transition of the fracture mode from a predominantly ductile to brittle nature. The particle marked by an arrow is identified as Al_2O_3

which provides stronger barrier to the motion of dislocation but offers less resistance to the advancing crack.

Conclusions

1. The CCT diagrams determined by dilatometric method demonstrated the role of Cu (1.5 wt%) and Ni (0.8 wt%) on the lowering of transformation start and finish temperatures of austenite under different cooling rates.
2. The Cu-containing alloys particularly at the higher cooling rates exhibit remarkable improvement in hardness.
3. The microstructure of the directly air-cooled 1.5 Cu–Ti–B steel comprised deformed proeutectoid ferrite and low temperature decomposition products of austenite without any perceptible amount of pearlite. 1.5 Cu–Ni–Ti–B steel resulted in a microstructure containing martensitic islands in ferrite matrix which closely resembles the microstructure of conventional ferrite–martensite dual phase steels. Transmission electron micrographs have evidenced significant amount of fine Cu precipitation (10–40 nm) in 1.5 Cu–Ti–B and 1.5 Cu–Ni–Ti–B steel formed during air-cooling.
4. Addition of Cu in Ti–B microalloyed steel improved the strength due to formation of precipitate during air-cooling of the hot-rolled steels. However, finer precipitates formed in the deformed ferrite pinned the dislocations and impaired ductility. In 1.5 Cu–Ni–Ti–B steel, the lowering of Ac_1 temperature and increasing amount of undeformed soft ferrite enhanced the ductility.
5. Addition of Cu resulted in the deterioration of impact properties particularly at sub-zero temperature due to pinning of dislocation formed in ferrite during hot rolling.

References

1. DeArdo AJ (1995) ISIJ Int 35(8):946
2. Davenport AT (ed) (1979) Formable HSLA and dual-phase steels. TMS-AIME, Warrendale, PA
3. Kot RA, Morris JW (eds) (1979) Structure and properties of dual-phase steels. TMS-AIME, Warrendale, PA
4. Kot RA, Bramfitt BL (eds) (1981) Fundamentals of dual-phase steels. TMS-AIME, Warrendale, PA
5. Shen XP, Priestner R (1990) Metall Trans 21A:2547
6. Wang XM, He XL (2002) ISIJ Int Suppl 42:S38
7. Navara E (1984) In: Dunne DP, Chandra T (eds) Proc. Int. Conf. on high strength low alloy steel. University of Wollongong, NSW, Australia, p 302
8. De Sy AL (1974) Trans Iron Steel Inst Jpn 14:139
9. Abe T, Kurihara M, Tagawa H, Tsukada K (1987) Trans Iron Steel Inst Jpn 27:478
10. Deschamps A, Militzer M, Poole WJ (2003) ISIJ Int 43(11):1826
11. ASM Metals Hand Book (1995) Properties and selection: iron; steels and high performance alloys, vol 1, 10th edn. ASM International, Materials Park, OH, p 389
12. Vander Voort GF (1984) Metallography principles and practice. McGraw Hill Book Company, New York, p 632
13. Shen Y, Hansen SS (1997) Metall Mater Trans A 28A:2027
14. Girault E, Jacques P, Harlet Ph, Mols K, Van Humbeeck J, Aernoudt E, Delannay F (1998) Mater Charact 40:111
15. Jacques PJ, Ladriere J, Delannay F (2001) Metall Mater Trans A 32A:2759
16. Jacques PJ, Girault E, Harlet Ph, Delannay F (2001) ISIJ Int 41(9):1061
17. Bainite Research Committee (1992) Atlas for bainitic microstructures, vol 1. ISIJ, Tokyo, p 97

18. Hollomon JH (1945) Trans AIME 162:268
19. Piplani RK, Raghavan V (1981) Steel India 4:1
20. Lian J, Jiang Z, Liu J (1991) Mater Sci Eng A147:55
21. Monteiro SN, Reed-Hill RE (1971) Met Trans 2:2947
22. Ramos LF, Matlock DK, Krauss G (1979) Metall Trans A 10A:259
23. Ludwik P (1909) Element der Technolnischen Mechanick. Julius Springer, Berlin, p 32
24. Byun TS, Kim IS (1993) J Mater Sci 28:2923. doi:10.1007/BF00354695
25. Skoufari–Themistou L, Crowther DN, Mintz B (1999) Mater Sci Technol 15:1069